13th ewtec 2019 Proceedings of the 13th European Wave and Tidal Energy Conference 1-6 Sept 2019, Naples, Italy

Development of WEC design loads: A comparison of numerical and experimental approaches

Brian J. Rosenberg, Tim R. Mundon, Ryan G. Coe, Eliot W. Quon, Chris C. Chartrand, Yi-Hsiang Yu, and Jennifer van Rij

***Abstract*—The development of accurate design loads is a critical part of the design of a wave energy converter. In this paper, we evaluate the extreme wave loading on the Triton WEC using a combination of mid-fidelity and high-fidelity numerical modeling tools, complemented by scaled physical model tests. The mid-fidelity approach used is a time-domain model based on linearized potential flow hydrodynamics, whereas the high-fidelity modeling tool is an unsteady Reynolds-averaged Navier Stokes computational fluid dynamics (CFD) model. A 1:30-scale physical model of the Triton WEC was tested at the Oregon State University Large Wave Flume. A comparison will be presented between the design loads predicted by the mid-fidelity model, the CFD model and the physical model tests, and based on this comparison, suggestions for best practices will be offered.**

***Index Terms*—wave energy converter (WEC), tank testing, time-domain numerical model, CFD, extreme response, design loads**

I. Introduction

FOR any wave energy converter (WEC), the development of accurate and reliable design loads is critical. Underestimation of loads will lead to component failure, whereas overestimation will result in increased structural costs and higher than necessary energy costs.

In this case study, we evaluate the design loads for a key structural component of the Triton WEC. Traditionally, this process would involve the development of a scaled physical model to ascertain the design loads for the environmental condition(s) of interest; however, the cost and complexity of constructing representative physical models is high, and it is becoming common to rely on numerical model representations to determine the structural loads. The rise in computational power make this increasingly more accessible; however, as with any model, simplifications and assumptions will have an impact on the representation of the full-scale system. It is important to consider the important trade-offs with this approach including accuracy of the hydrodynamics, accuracy of the extreme wave forcing, and efficiency (speed) of the simulation or experiment.

Paper 1682 - Wave Device Development and Testing
B. J. R. and T. R. M. are with Oscilla Power, Inc., Seattle, WA, U.S.A. (e-mail: rosenberg@oscillapower.com, mundon@oscillapower.com).
R. G. C. and C. C. C. are with Sandia National Laboratories, Albuquerque, NM, U.S.A.
E. W. Q., Y. Y. and J. V. R. are with the National Renewable Energy Laboratory, Golden, CO, U.S.A.

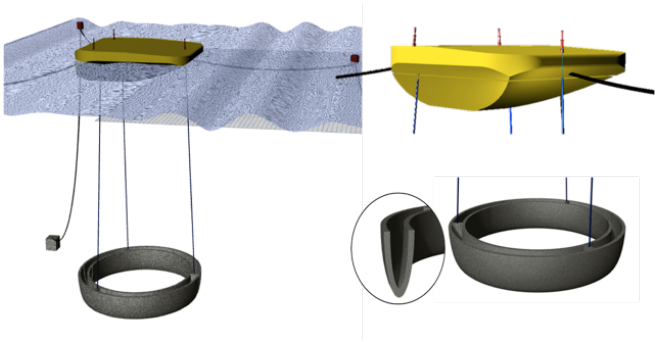

Fig. 1. Illustration of the Triton WEC.

A. Study device

In this case study, we examine extreme wave loading on the Triton WEC, a 1-MW-rated two-body quasi point absorber under development by Oscilla Power, Inc. (OPI). A diagram of the device in operational mode is shown in Fig. 1. The device is composed of two bodies: a surface float and a submerged reaction ring structure, coupled together by three flexible tendons. In this study, we are interested in the maximum design loads for the tendons during a hypothetical deployment off the U.S. West Coast.

As the surface float is excited by the wave resource, the two bodies move and react relative to each other and the resulting tension variations in each tendon drive three separate power-take-off (PTO) systems housed inside the surface float. Due to the three separate tendons and PTO systems, energy is captured from all degrees of relative motion in translation and rotation.

Each of the three tendons attaches to an independent linear drivetrain that consists of two elements: a "return spring" and a generator. The operation of the drivetrain is described in further detail by [1]. The return spring supports the mean underwater weight of the reaction ring, keeping the mean PTO position at the center of travel. The associated spring rate is approximately linear and can be varied based on the sea state as a tuning parameter. While the drivetrain is capable of implementing advanced control strategies, for simplicity, this study will employ a proportional damping strategy where the drivetrain is approximated to a linear spring and damper, respectively. The corresponding spring and damping coefficients are

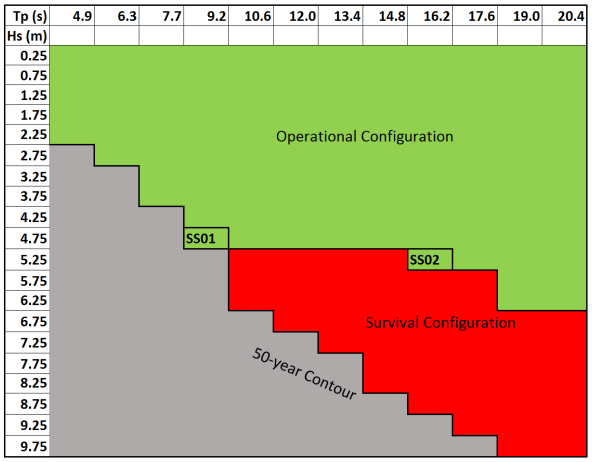

Fig. 2. Sea state contour denoting selected design sea states.

TABLE I
DESIGN WAVES

Sea State ID	T_p [s]	H_s [m]	$H_{regular}$ [m]
SS01	9.2	4.75	9.0
SS02	16.2	5.25	9.9

selected to maximize power capture in each state [2] with the added constraints that it must avoid end-stop impacts and the tendons must remain taut.

As shown in Fig. 1, the WEC is kept on station using a three-point catenary mooring. Each mooring leg comprises an upper line segment, attached to a surface float, and a lower line segment, anchored to the seafloor. This arrangement provides compliant horizontal stationkeeping while providing minimal vertical forces on the WEC.

B. Design wave conditions

A first step in the design process is identifying the environmental condition(s) that drive the maximum load for the component in question [3], [4].

In this study, we are interested in the maximum design loads for the tendons during a hypothetical Triton deployment off the coast of California (U.S. Department of Energy Humboldt Bay reference location). The design envelope was selected to be the 50-year wave contour, where significant wave heights (H_s) can reach up to approximately 10 m in extreme sea states [5]. However, in sea states where H_s is larger than approximately 5 m, the WEC reconfigures through ballasting from the "operational" configuration (Fig. 1) and enters a different "survival" configuration in order to improve device survivability at the expense of reduced power capture.

In this load-shedding configuration, dynamic tendon loads are greatly reduced and the consequence is that the maximum tendon loads are driven by the largest waves in which the device is in the operational configuration. The maximum operational contour then becomes a design choice and is selected here to be in the vicinity of $H_s \leq 5$ m based on various system constraints. Specifically, this design wave contour was selected to prevent end-stop events on the PTO travel and slack events in the tendons. This maximum operational contour was identified by running a series of simulations using a midfidelity model to identify the area within the design wave envelope that the system may be safely operated without experiencing these events [6].

From the results of these midfidelity simulations, two design-load-case sea states of interest were identified (SS01 and SS02). Sea state SS01 results in the largest tendon loads, whereas sea state SS02 elicits a slightly lower magnitude response but provides another data point along the extreme operational contour. The H_s and peak wave period, T_p, for these two sea states are summarized in Fig. 2 and Table I.

II. NUMERICAL METHODS

Two numerical models were developed for the full-scale Triton: a midfidelity time-domain model based on linearized potential flow hydrodynamics, and a high-fidelity computational fluid dynamics (CFD) model.

C. Midfidelity model

For WEC evaluation in performance (energy production) waves, linear models such as those based on the hydrodynamics from a boundary element model (BEM), are typically utilized. In this study, we used a model in which the multibody dynamics for the coupled marine and PTO systems of the Triton WEC were solved in the time domain using the commercial marine dynamics software Orcina OrcaFlex [6], [7].

For the surface float, the frequency-dependent added mass, damping, and linearized excitation forces were computed using the BEM solver Nemoh [8]. The line dynamics for the tendons and moorings were solved in OrcaFlex using lumped mass finite elements, and the PTOs were modeled by three linear spring-damper elements connected between the surface float and the top of each tendon. The reaction ring, which interacts minimally with the free surface, was modeled using a bulk Morison formulation in each degree of freedom. The hydrodynamic contributions to the reaction ring force, in the form of added mass and viscous drag, have been studied and quantified using CFD and laboratory experiments [9].

D. CFD model

In large waves, the assumption of linear hydrodynamics breaks down, and a more accurate numerical formulation for the prediction of extreme design loads is offered by CFD models; however, there are some limitations. While CFD models offer more accurate hydrodynamics calculations, the complexities of simulating multi-body WEC systems near the free surface with complex subsystem dynamics (e. g., PTO control and mooring systems) have limited the application of CFD to WECs.

As a first-order approximation, the Triton mooring arrangement can be represented by an equivalent linear horizontal spring stiffness and pretension acting at

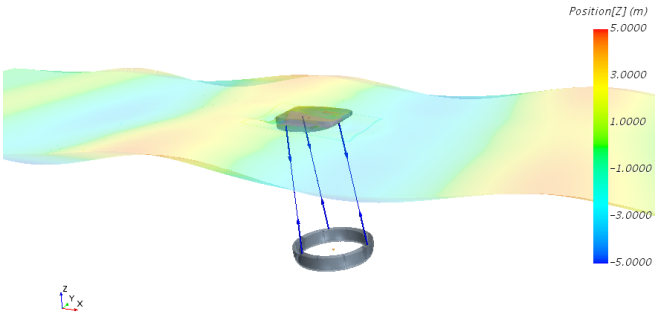

Fig. 3. Rendering of SS01-R regular wave case ($H = 9.0\,\text{m}$ and $T = 9.2\,\text{s}$) from [6].

the surface float center of gravity. This linear mooring model will be used for the CFD simulations presented in this study, whereas the full mooring line dynamics were solved using a finite element representation in the midfidelity OrcaFlex simulations. Future work might involve coupling the CFD software to an external mooring model such as OrcaFlex.

A CFD model of the Triton device was developed with complete details specified in [6]. The commercial software package STAR-CCM+ was used to model the Triton device. In this case, STARCCM+ solves the unsteady Reynolds-averaged Navier-Stokes (RANS) equations using a finite volume spatial discretization and a $k-\omega$ turbulence model. A volume of fluid (VOF) approach was used to accommodate the multiphase free surface flow.

To capture the motion of the two-body Triton device, an overset mesh approach was utilized [10], [11]. In this arrangement, the computational domain was split into three regions: a background region that includes the bulk of the domain, an overset region that tracks the motion of the float, and an overset region that tracks the motion of the reaction ring. Each region remains rigid and the solution for the fluid simulation is passed between the regions via interpolation. This approach was chosen over alternatives, such as mesh morphing/deformation and sliding interfaces, for its flexibility and its ability to maintain good mesh resolution even in cases of large amplitude motion.

Meshing within the computational domain was configured based on a number of factors. The mesh at the free surface is of particular importance, where the mesh was prescribed such that $\lambda/\Delta x > 100$ and $H/\Delta z > 40$. Here, λ is the wave length and H is the wave height. The cell spacing is defined in the wave propagation and vertical directions by Δx and Δz, respectively. Time steps were chosen based on the Courant-Friedrichs-Lewy (CFL) number, both in the traditional velocity formulation but also in formulations considering the movement of the free surface.

To handle the tendon linkages between the two bodies and the PTOs, a series of custom functions were defined. The functions use the spring and damper coefficients of the PTO and a simple vector force formulation. The mooring system is handled similarly. It should be noted that catenary effects and slack-line conditions are not well-captured by this formulation.

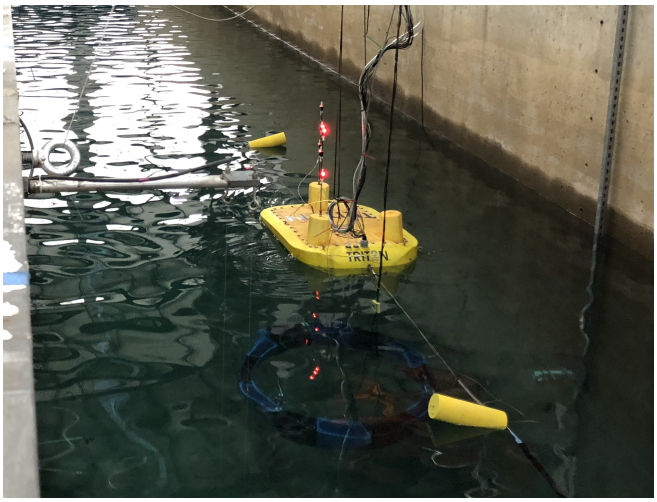

Fig. 4. 1:30 physical model of Triton WEC in still water at the Oregon State University Large Wave Flume.

III. Physical Model

In addition to the numerical models described above, a 1:30 Froude-scaled model of the Triton was built and tested at the Oregon State University (OSU) Large Wave Flume (Fig. 4).

E. Construction

To achieve a high degree of geometric similarity and strength, the surface float was 3D-printed as a hollow shell and reinforced with an outer layer of fiberglass and epoxy. High-density inserts were incorporated to serve as interfaces for mounting the PTO and mooring lines. The reaction ring was 3D-printed from 12 ABS plastic sections that are bolted together and lead ballasted.

The float was fitted with a sealed top hatch to eliminate water ingress during testing and to allow the internal PTO to be accessed and modified between tests. Due to the numerous hull penetrations, namely the access hatch and the pressure transducers, a positive pressure system was incorporated in the surface float to keep its internal air pressure of ~ 5 psig, thus preventing water ingress.

F. Representative PTO

The 1:30 Triton model contained three representative PTOs housed inside the surface float—one for each of the three tendons (Fig. 5 and 6). Three bellmouth fairleads, 3D-printed from a self-lubricating material, were incorporated into the surface float to align each tendon (2 mm UHMWPE) with each PTO. Each PTO comprises a spring-damper element consisting of an extension spring to support the weight of the reaction ring, and an adjustable rotary oil dashpot, to represent the power absorption (generator). This arrangement is conceptually similar to the full-scale drivetrain, and the spring and oil damper were selected such that they provide similar characteristics as the full-scale Triton drivetrain.

The linear displacement and force exerted by the relative motion of the reaction ring and surface float

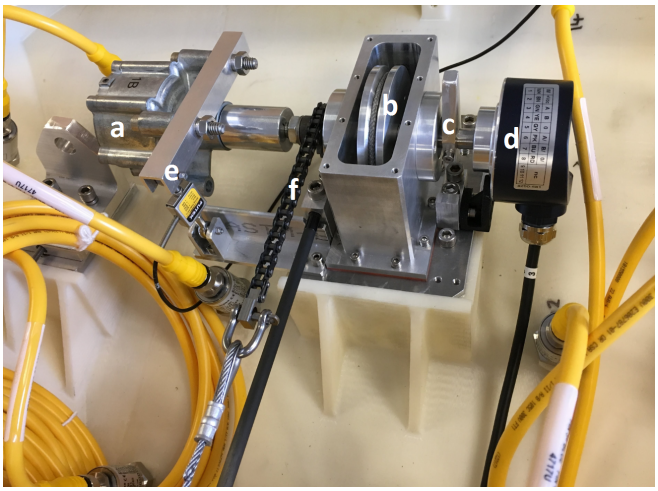

Fig. 5. Physical model PTO inside the hull: (a) rotary oil damper, (b) tendon wrapping over sheave, (c) end-stop cam, (d) encoder, (e) damper torque arm and load cell, and (f) sprocket-chain assembly.

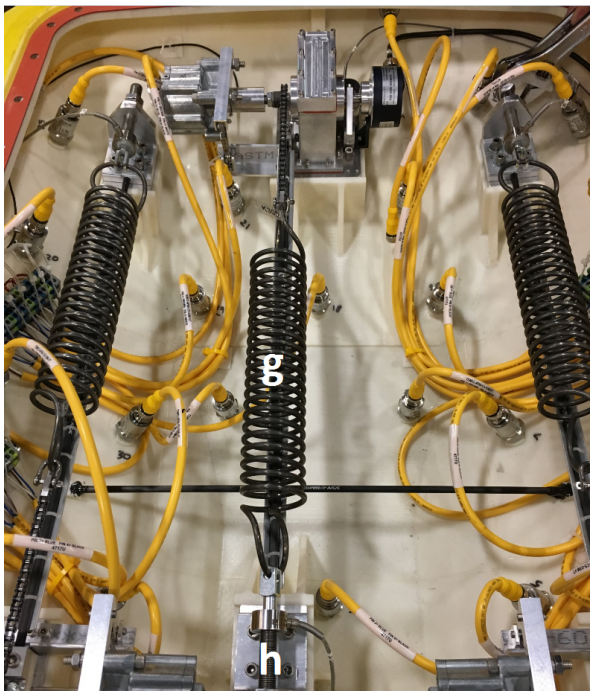

Fig. 6. Physical model PTO inside the hull: (g) extension spring and the (h) spring load cell.

is translated to rotary motion by the tendon wrapping once around a sheave. The rotary oil damper (Kinetrol S-CRD) is directly attached to the sheave's axle. This unit dissipates energy by shearing viscous fluid (silicone oil) between the rotor and stator discs. A chain/sprocket assembly is used to convert the sheave rotary motion back into linear motion for the extension spring.

The physical model spring and damping profiles (both converted to an equivalent force and displacement effective in line with the tendon) are presented in Fig. 7 and Fig. 8, along with the "target" linear profiles used in the CFD and OrcaFlex models. These experimental profiles were obtained directly from physical model measurements during an irregular wave test.

The physical model PTO spring stiffness was within

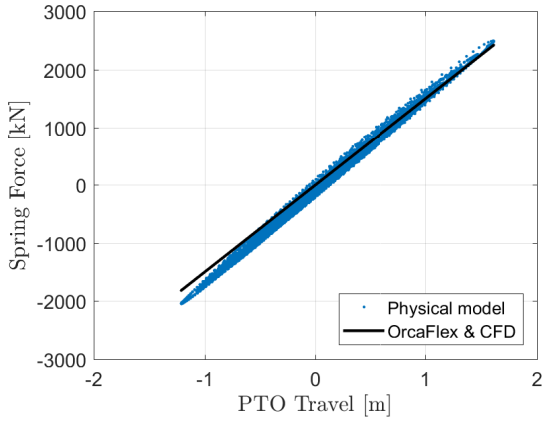

Fig. 7. PTO spring component for the physical model compared to the target profile. All results correspond to the force-displacement profile effective at the tendon. Physical model profile obtained from Test SS01-I-EXP, where each data point represents an instant in time.

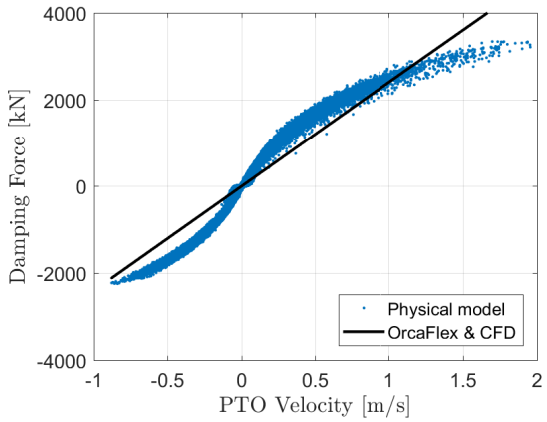

Fig. 8. PTO damping component for the physical model compared to the target profile. All results correspond to the force-velocity profile effective at the tendon. Physical model profile obtained from Test SS01-I-EXP, where each data point represents an instant in time.

7% of the target value, as shown in Fig. 7. The physical model damper is slightly nonlinear, as shown in Fig. 8, with a higher damping at low speeds and lower damping at high speeds, though the mean damping coefficient is in line with the target value.

The full-scale Triton WEC has mechanical end stops imposed by the input hydraulic cylinders that limit the tendons' linear travel. Representative hard end stops in the 1:30 model are provided by a cam mechanism attached to the sheave axle. After the sheave revolves $\pm$ 95 degrees (equivalent to the full-scale system travel limitation), the cam hits a elastomeric bumper, causing the PTO motion to be restrained. This end impact force was measured by a load cell underneath the bumper.

G. Representative mooring

Due to the width of the OSU flume, the laboratory mooring was modified from a three-point configuration to a two-point (bow and stern) configuration. An additional contributing factor to the laboratory mooring design was that the OSU flume was representative of an 80-m depth (flume still water depth = 2.7 m),

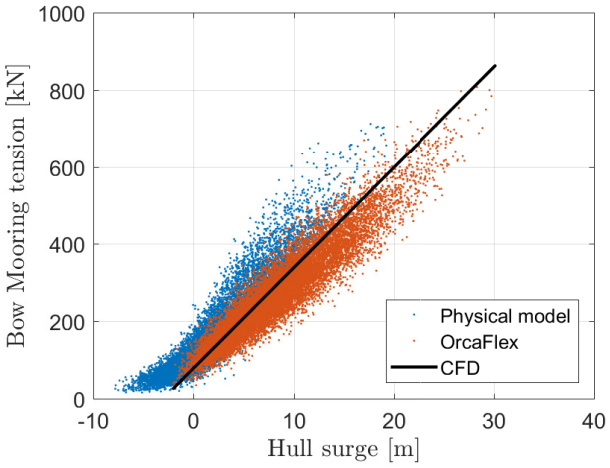

Fig. 9. Mooring profile as a function of WEC surge displacement, where 0 represents the WEC equilibrium position. Experimental profile obtained from Test SS02-I-EXP, OrcaFlex profile obtained from SS02-I-OFX. Each data point represents an instant in time. The solid line represents the linear mooring model used for CFD obtained from static offset tests using the OrcaFlex model.

whereas the numerical simulations in this project were performed for a 120-m berth.

Careful attention was given to ensure that the laboratory mooring provided a similar effective stiffness as the realistic arrangement. In order to maintain a consistent mooring scope in the laboratory arrangement, the lower mooring line was shortened and the anchor radius reduced. A separate OrcaFlex instance was then used to model this laboratory mooring arrangement and to determine an appropriate line elasticity that would give an equivalent mooring force-displacement profile as the realistic mooring arrangement. Appropriate mechanical springs were then selected and introduced in the upper and lower lines for the 1:30 model tests.

Figure 9 shows the mooring force-displacement curve obtained from the physical model (i.e., two-point mooring, 80-0m depth) compared to the full-scale arrangement in OrcaFlex (i.e., three-point mooring, 120-m depth), both profiles obtained from a long duration irregular wave test. Also plotted is the linear mooring model used in the CFD simulations. This profile was obtained from static offset tests using the OrcaFlex model. Given the challenges in perfectly representing the full-scale system in the laboratory, the agreement is reasonable.

H. Instrumentation

Four measurements of wave elevation were made using resistive wave gauges: two upwave of the WEC, one at the WEC location, and one downwave of the WEC. The wave probes were positioned 35 cm away from the basin sidewalls due to the acceptable lateral uniformity of the waves. These wave probes were in place during device testing and calibration (no device in flume). Wave calibrations were performed prior to model testing to ensure accuracy of wave period and wave height to within 5%. All waves were tested at 0 incidence to the physical model (waves travel right to left in Fig. 1 and 3, and top to bottom in Fig. 4).

TABLE II
TEST CONDITIONS

ID	Sea State	Wave Type	Model
SS01-I-EXP	SS01	Irregular	Physical model
SS01-I-OFX	SS01	Irregular	OrcaFlex
SS01-R-EXP	SS01	Regular*	Physical model
SS01-R-CFD	SS01	Regular	CFD
SS01-F-EXP	SS01	Focused	Physical model
SS01-F-CFD	SS01	Focused	CFD
SS02-I-EXP	SS02	Irregular	Physical model
SS02-I-OFX	SS02	Irregular	OrcaFlex
SS02-R-EXP	SS02	Regular	Physical model
SS02-R-CFD	SS02	Regular	CFD

* For tests marked "regular", an equivalent monochromatic wave was run with $H = 1.9H_s$ for the corresponding irregular sea state.

The physical model contained three optical rotary encoders to measure the angular displacement of each of the sheaves. Load cells were used to measure each of the PTO spring forces and damping torques, as indicated in Fig. 5. Load cells underneath the end-stop bumpers were used to assess end-stop impacts. Submersible load cells were also placed in line with each of the three tendons and both of the mooring lines.

A six-degrees-of-freedom motion capture of the surface float was performed using the OSU PhaseSpace system, and an IMU was installed on the reaction ring structure to measure its motion. All motion, instrumentation, and wave data were sampled on a concurrent time basis at 100 Hz (model scale).

IV. DESIGN WAVE REPRESENTATIONS

In order to assess the maximum load for the component in question, a typical approach is to evaluate the device response in a realistic irregular sea state until statistical convergence is observed—guidance is approximately 3 hours [12]. In this study, both the physical model and the midfidelity OrcaFlex model can be efficiently run in irregular waves to achieve statistical convergence of the Triton tendon loads.

Due to the impractically long computational times required for a similar convergence in CFD, the process for assessing design loads, similar to that used in [13], was applied. For the sea states of interest (SS01 and SS02), two simplified design-wave approaches were evaluated: regular (monochromatic) waves and focused (most likely extreme response) waves. These simplified design wave approaches aim to capture the extreme response of the WEC within a feasible amount of computational effort.

For sea states SS01 and SS02, a regular wave of height, $H_{regular} = 1.9H_s$, was used to approximate the largest individual wave, and therefore the largest device response within the corresponding irregular sea. The factor of 1.9 comes from the common assumption of wave amplitudes following a Rayleigh distribution.

The focused wave approach involves exciting the WEC with a broadband impulse. Here, the OrcaFlex

simulation results were used to produce wave and response spectra for the quantity of interest (i.e., tendon tension), and from these responses, the most likely extreme response (MLER) method was used to develop a corresponding focused wave [6], [14]. As sea state SS01 produced the largest tendon tension (which occurred in the bow tendon), the MLER wave SS01-F was generated to excite this response.

Table II summarizes the tests evaluated in this study. The test matrix considers the three different models (OrcaFlex, CFD, physical model) and the three different wave representations (irregular, regular, focused). As a validation measure, the three CFD cases were replicated in the physical model tank tests.

To achieve well-converged statistics from the OrcaFlex simulations, six independent realizations of each sea state were run, wherein each realization had a unique phase distribution for the constitutive wave components. The duration of each simulation was 3 hours and the time step was $\Delta t = 0.005\,\mathrm{s}$. A Bretschneider wave spectrum was used for all irregular wave tests.

V. Results

For physical model test SS01-I-EXP, the irregular wave test was executed twice, first for a full-scale equivalent of approximately 1 hour and then for an equivalent of approximately 2 hours, where each run consisted of a unique wave elevation time series. The maximum bow tendon tension observed for the two different runs is different by only 4%, demonstrating that the maximum load is well-converged statistically and that very high percentile responses have been observed.

As shown in Fig. 10, for both tests, the bow tendon remains taut and the peak-to-peak PTO travel remains within its 3 m limitation (all quantities are presented with respect to the full-scale device). Therefore, the results are not corrupted by slack tendon events or end-stop events. Similarly, test SS02-I-EXP did not exhibit these events. Figure 10 shows that both the minimum tendon tension and the maximum PTO travel are near their limitations. This validates previous midfidelity modeling work that suggests that this sea state (SS01) is near the wave height threshold at which the system can safely remain on the surface without experiencing potentially harmful slack events and end-stop events, as denoted by the maximum operational contour in Fig. 2).

I. *Comparison between experiments and CFD*

To validate the accuracy of the CFD model, the three CFD cases listed in Table II were replicated using the physical model.

Figure 11 compares the physical model and CFD data for focused wave case SS01-F. The results demonstrate that the peak tendon tension for the CFD simulation and tank test agree to within 7%.

Figure 12 compares the physical model and CFD data for regular wave case SS01-R. In this wave condition, the physical model exhibited slack events

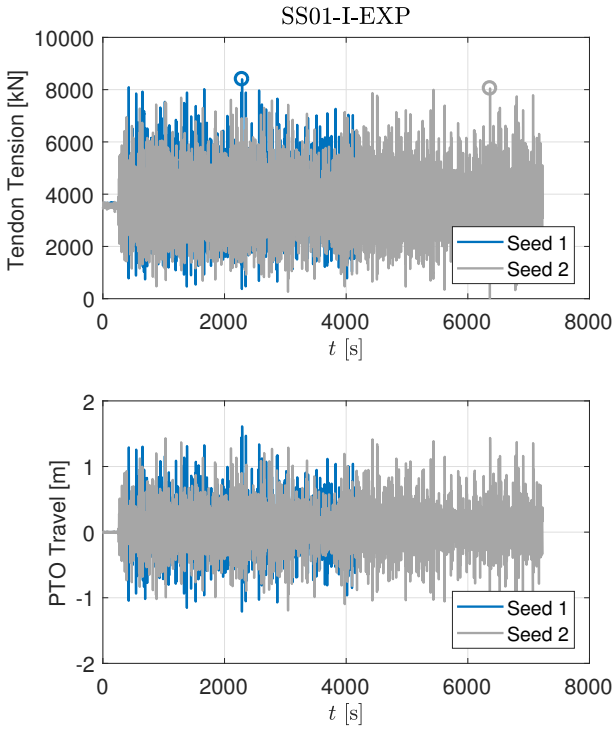

Fig. 10. Physical model irregular wave test SS01-I-EXP.

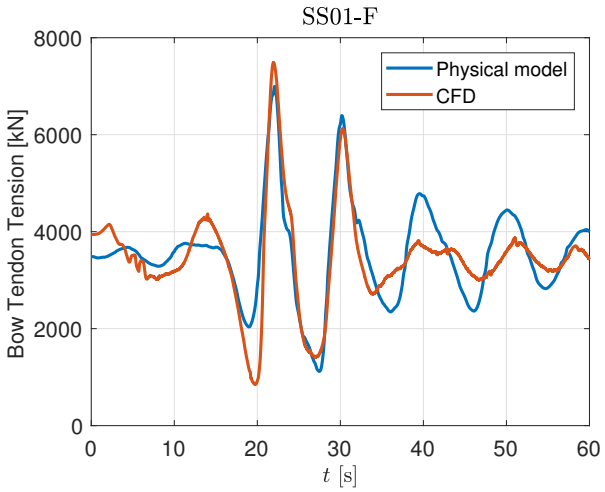

Fig. 11. Comparison between experiments and CFD for focused wave SS01-F.

and end-stop impacts, which result in significant load spikes. These effects are not implemented in the CFD framework; however, the tendon remains taut in this simulation. Removing the end-stop load component from the tendon tension time series suggests reasonable agreement between the physical model and CFD; however, this physical model test will not be considered in subsequent analysis as these events may have impacted the WEC dynamics.

Figure 13 compares the physical model and CFD data for the regular wave case SS02-R. This demonstrates that the peak tendon tension in the CFD simulation and tank test agree to within 10%.

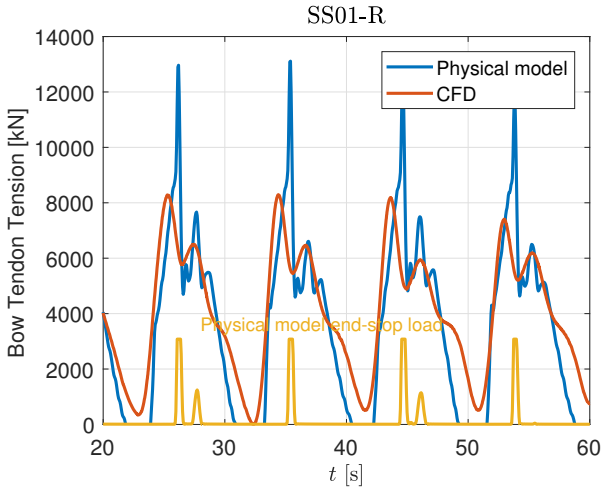

Fig. 12. Comparison between experiments and CFD for regular wave SS01-R.

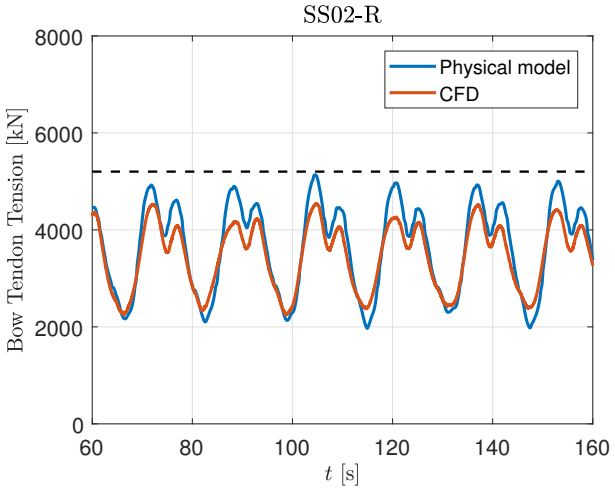

Fig. 13. Comparison between experiments and CFD for regular wave SS02-R.

TABLE III
MAXIMUM BOW TENDON LOAD FOR EACH TEST CONDITION.

Test	Maximum Bow Tendon Load [MN]	% Difference
SS01-I-EXP	8.40	0.0
SS01-I-OFX	8.76	4.3
SS01-R-EXP	*	*
SS01-R-CFD	8.27	-1.5
SS01-F-EXP	7.00	-17
SS01-F-CFD	7.49	-11
SS02-I-EXP	7.22	0.0
SS02-I-OFX	7.16	-0.8
SS02-R-EXP	5.14	-29
SS02-R-CFD	4.73	-34

* This test is not included because slack tendon events and end-stop events were excited; therefore, the overall WEC dynamics may have been modified.

J. Comparison of design loads for each method

Table III and Fig. 14 summarize the maximum bow tendon load produced by all experimental and numerical approaches. Percent differences for each method are compared to the equivalent long-duration irregular physical model test, which is taken here to be the benchmark.

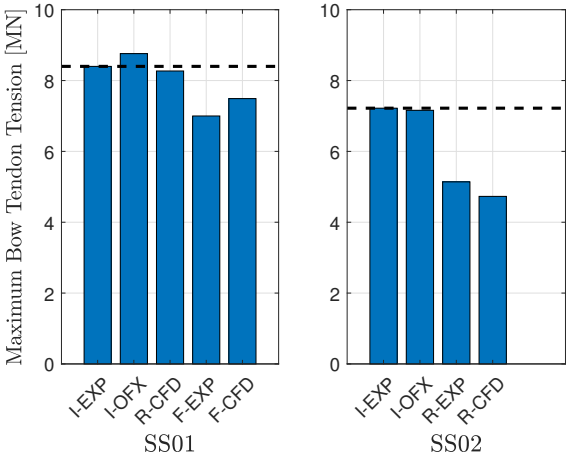

Fig. 14. Comparison of maximum bow tendon tension for all numerical and physical approaches. The dashed line represents the maximum load observed in the long-duration irregular wave physical model tests.

Of the numerical methods, the midfidelity OrcaFlex model fared the best. The maximum tendon load was accurate to within 5% for both sea states SS01 and SS02.

The focused wave approach produced a high percentile response load, though it underpredicted the design load by 17% and 11% for the physical model tests and CFD simulation, respectively, in sea state SS01.

The design loads produced from the regular wave approach had varying levels of accuracy. For sea state SS01, the maximum tendon tension was reliably predicted by the CFD model to within 2%. However, for sea state SS02, the load was underpredicted by 29% and 34% for the physical model test and CFD simulation, respectively.

VI. CONCLUSIONS

One aim of this study was to examine the accuracy and trade-offs of using a high-fidelity nonlinear hydrodynamics model with simplified wave forcing (CFD) versus using a linearized hydrodynamics model with fully-converged device statistics in a long-duration irregular sea state (midfidelity model).

The results suggest that, at least for the wave conditions evaluated here, the midfidelity OrcaFlex model provides more consistently accurate results in this application, even though the waves investigated are rather large, such that we might expect nonlinear effects to be non-negligible. The OrcaFlex model, while relying on linearized hydrodynamics, can implement long-duration irregular waves within a reasonable computational effort; therefore, long-duration statistics can be realized.

The varying levels of accuracy between the design loads produced by CFD and the long-duration irregular physical model tests could be attributed to two explanations: inaccuracies in the CFD calculation, or inability of the simplified design waves to reliably predict the maximum loads in the corresponding irregular sea state. The results from this study indicate

that the CFD model compares fairly well against the physical model tests, suggesting that the simplified wave approaches have some shortcomings. For example, in Test SS02-R, although the CFD simulation and physical model test agree to within 10%, the design loads measured are approximately 30% below those achieved in the long-duration irregular tank test.

In this respect, another aim of this study was to determine if the simplified wave approaches (i.e., regular and focused waves) are good proxies for long-duration irregular wave tests, and if the device load responses are similar. The simplified wave approaches are interesting for two reasons. First, CFD is unable to efficiently handle long-duration irregular wave simulations, and these simplified wave approaches enable high-fidelity CFD to be used in extreme design load analysis (where hydrodynamics tend to be nonlinear). Second, these wave representations aim to excite a large device response in a short period of time. A focused wave test may take just a few seconds in the laboratory and a regular wave test may take a few minutes in the laboratory (assuming several wave cycles are conducted to reach steady-state response). If a WEC design load may be accurately inferred from a short duration test, that would be benefit the design process, as it would allow physical model test campaigns to be run more efficiently.

While the regular wave approach showed varying levels of accuracy in this application, it predicted the design load very accurately for one sea state. Further research is needed to investigate the reasons for the discrepancy and to find potential ways to improve the approach. Furthermore, the focused wave approach appears promising, as it produced a design load response within 17% of the response in a realistic irregular wave. This approach may also be further refined to improve accuracy.

ACKNOWLEDGEMENT

This material is based upon work supported by the U.S. Department of Energy under Award Number DE-EE0007346.

Sandia National Laboratories is a multi-mission laboratory managed and operated by National Technology and Engineering Solutions of Sandia, LLC., a wholly owned subsidiary of Honeywell International, Inc., for the U.S. Department of Energy's National Nuclear Security Administration under contract DE-NA0003525.

This work was also authored by the National Renewable Energy Laboratory, operated by Alliance for Sustainable Energy, LLC, for the U.S. Department of Energy (DOE) under Contract No. DE-AC36-08GO28308. Funding for this work was provided by the U.S. Department of Energy Office of Energy Efficiency and Renewable Energy Wind Energy Technologies Office. The views expressed in the article do not necessarily represent the views of the DOE or the U.S. Government. The U.S. Government retains and the publisher, by accepting the article for publication, acknowledges that the U.S. Government retains a nonexclusive, paid-up, irrevocable, worldwide license to publish or reproduce the published form of this work, or allow others to do so, for U.S. Government purposes.

REFERENCES

[1] T. Mundon, B. Rosenberg, and V. J., "A hybrid drivetrain for low-speed, linear WEC applications," in *5th Marine Energy Technology Symposium (METS)*, Washington, D.C., 2016.

[2] C. Liang and L. Zuo, "On the dynamics and design of a two-body wave energy converter," *Renewable Energy*, vol. 101, pp. 265–274, 2017.

[3] R. G. Coe, Y.-H. Yu, and J. van Rij, "A survey of WEC reliability, survival and design practices," *Energies*, vol. 11, no. 1, p. 4, 2018. [Online]. Available: http://www.mdpi.com/1996-1073/11/1/4

[4] IEC, "Marine energy - wave, tidal and other water current converters - part 2: Design requirements for marine energy systems," International Electrotechnical Commission (IEC), August 2016. [Online]. Available: https://webstore.iec.ch/publication/25634

[5] A. Dallman and V. Neary, "Characterization of U.S. wave energy converter (WEC) test sites: A catalogue of met-ocean data," Sandia National Laboratories, Tech. Rep. SAND2014-18206, 2014.

[6] R. Coe, B. Rosenberg, E. Quon, C. Chartrand, Y.-H. Yu, J. van Rij, and T. Mundon, "CFD design load analysis of a two-body wave energy converter," *Journal of Ocean Engineering and Marine Energy, in press*, 2019.

[7] OrcaFlex, *OrcaFlex Manual*, Orcina Ltd., Daltongate Ulverston Cumbria, UK, 2015.

[8] A. Babarit and G. Delhommeau, "Theoretical and numerical aspects of the open source BEM solver NEMOH," in *11th European Wave and Tidal Energy Conference (EWTEC2015)*, 2015.

[9] T. R. Mundon, B. J. Rosenberg, and J. van Rij, "Reaction body hydrodynamics for a multi-dof point-absorbing WEC," in *12th European Wave and Tidal Energy Conference (EWTEC2017)*, 2017.

[10] J. H. Ferziger and M. Peric, *Computational methods for fluid dynamics*. Springer Science & Business Media, 2012.

[11] I. Hadzic, J. Hennig, M. Peric, and Y. Xing-Kaeding, "Computation of flow-induced motion of floating bodies," *Applied Mathematical Modelling*, vol. 29, no. 12, pp. 1196–1210, Dec. 2005.

[12] M. K. Ochi, *Ocean Waves: The stochastic approach*. Cambridge University Press, 2005, vol. 6.

[13] J. van Rij, Y.-H. Yu, and R. G. Coe, "Design load analysis for wave energy converters," in *37th International Conference on Ocean, Offshore and Arctic Engineering (OMAE2018)*, Madrid, Spain, 2018.

[14] E. Quon, A. Platt, Y.-H. Yu, and M. Lawson, "Application of most likely extreme response method for wave energy converters," in *35th International Conference on Ocean, Offshore and Arctic Engineering (OMAE2016)*, Busan, Korea, 2016.